EFFICIENT STRUCTURE-AWARE 3D GAUSSIANS VIA LIGHTWEIGHT INFORMATION SHAPING

Anonymous authors
Paper under double-blind review

ABSTRACT

3D Gaussians, as an explicit scene representation, typically involve thousands to millions of elements per scene. This makes it challenging to control the scene in ways that reflect the underlying semantics, where the number of independent entities is typically much smaller. Especially, if one wants to animate or edit objects in the scene, as this requires coordination among the many Gaussians involved in representing each object. To address this issue, we develop a mutual information shaping technique that enforces resonance and coordination between correlated Gaussians via a Gaussian attribute decoding network. Such correlations can be learned from putative 2D object masks in different views. By approximating the mutual information with the gradients concerning the network parameters, our method ensures consistency between scene elements and enables efficient scene editing by operating on network parameters rather than massive Gaussians. In particular, we develop an effective contrastive learning pipeline with lightweight optimization to shape the attribute decoding network, while ensuring that the shaping (consistency) is maintained during continuous edits, avoiding re-shaping after parameter changes. Notably, our training only touches a small fraction of all Gaussians in the scene yet attains the desired correlated behavior according to the underlying scene structure. The proposed technique is evaluated on challenging scenes and demonstrates significant performance improvements in 3D object segmentation and promoting scene interactions, while inducing low computation and memory requirements. Our code and trained models will be made available.

1 INTRODUCTION

Open-world 3D scene understanding and editing play important roles in gaming, AR/VR, and robotics applications. Recently, 3D Gaussian Splatting (3DGS) (Kerbl et al., 2023), has significantly advanced both the rendering quality and inference efficiency in 3D learning by representing scenes through a set of 3D Gaussians. Moreover, follow-up works in scene editing (Cen et al., 2023; Zhou et al., 2023; Ye et al., 2023) propose augmenting each Gaussian's parameters with task-relevant attributes, allowing users to edit scenes by selecting Gaussians based on these attributes and modifying their colors or positions. Despite the progress with 3DGS-based scene editing, the use of point-wise 3D Gaussians presents limitations, among which, the fact that the number of distinct and interactive entities in a scene is typically far fewer than the number of Gaussians is neglected. Furthermore, augmenting attributes of Gaussians introduce significant storage overhead and do not fundamentally address the lack of correlation between Gaussians.

The lack of intrinsic correlation among scene elements renders a clear contrast between the editing of 3D Gaussians and the perturbation in the real world. For example, real-world scenes consist of particles that aggregate into cohesive objects through physical or chemical bonds, forming highly organized, interdependent structures. Interactions with a small part of an object can induce changes throughout the entire entity due to these intrinsic correlations. Such a phenomenon implies a high degree of mutual information between particles of the same entity, and even across distinct objects. Ideally, 3D scene representations should capture these correlation structures, facilitating efficient learning and interaction for tasks like scene editing. If so, modifying the state of a single element could result in coherent adjustment in the states of all correlated elements, which promotes efficiency by eliminating the need to individually examine and edit each Gaussian.

To enable efficient object-level interactive tasks, we propose the key is to enforce the inherent correlation structure within the scene representation, with which, the propagation of changes across

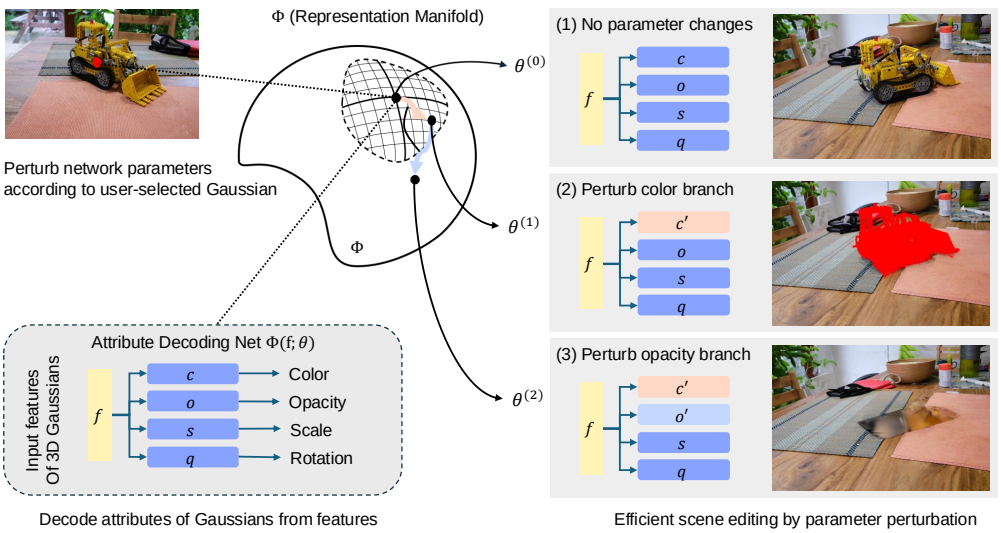

Figure 1: The proposed mutual information shaping of the attribute decoding network based on 3D Gaussian Splatting Kerbl et al. (2023) can capture the underlying structure of the scene, while maintaining the correlations after consecutive parameter changes according to user-selected Gaussian (specified in Sec. 3.7). It promotes efficient scene editing by perturbing the network parameters, including re-colorization, segmentation, object removal, etc.

correlated Gaussians can be easily achieved. Instead of assigning additional attributes to each Gaussian for grouping purposes, we introduce a novel learning scheme that encodes the correlations into the representation and an effective approach for manipulating scene. Note that, a few 3DGS-based compression methods have exploited similarities between Gaussians to reduce storage cost, such as clustering Gaussians with similar parameter values (Fan et al., 2023), introducing anchors to group nearby Gaussians in different spatial regions (Lu et al., 2023), or organizing 3D space with feature closeness (Chen et al., 2024). These techniques primarily target scene reconstruction and rendering, however, we propose an explicit modeling of the correlations from the perspective of mutual information maximization to enable efficient scene editing.

We develop upon the common practice of 3DGS compression methods, where Gaussian attributes (used for reconstruction) are decoded from their features, and we introduce a mutual information shaping scheme to explicitly enforce the correlations between Gaussians via the feature-decoding network. This scheme ensures that perturbing the network parameters results in coherent changes among correlated Gaussians, enabling controllable and semantically meaningful interactions with objects in the rendered scene. Our strategy circumvents the need to estimate and encode pairwise feature correlations among millions of Gaussians. Instead, it constructs a well-organized tangent space that captures the underlying structure of the scene within the network.

Specifically, we devise a shaping loss that maximizes the mutual information (MI) between Gaussians belonging to the same entity (as evidenced by putative metrics), which correlates Gaussians associated with the same object and de-correlates otherwise. Furthermore, mutual information between Gaussians is approximated by the cosine similarity between the Jacobians with respect to the perturbed weights. This legitimates the tangent space of the feature-decoding network parameters to encode the desired correlation structure. However, simply shaping the tangent space *does not* guarantee that the perturbed network will preserve this correlation structure when the shaped weights are modified, i.e., the after-modification parameters may not have a shaped tangent space, thus, making it incapable of consistent perturbations across multiple editing operations. Another challenge lies in the computational and memory overhead required to calculate Jacobians, as this necessitates storing the full computational graph regarding the derivative of the Jacobians – a significant cost for 3DGS, where storage and training efficiency are critical concerns.

To further overcome these challenges, we propose shaping the activations of the perturbed weights instead of the Jacobians. We prove that this technique ensures that the network undergoes a conformal transformation in its tangent space, maintaining the correlation structure and enabling consistent editing across sequential operations. In other words, the proposed is a sufficient condition for mutual information maximization while inducing the benefits not possessed by directly shaping Jacobians. Finally, we develop an efficient pipeline that shapes the feature-decoding network with consistency preserved along a sequence of perturbations, while being computationally efficient. This pipeline is fully automated and light-weight. We evaluate the proposed MI shaping technique across various scene-editing applications, including 3D object removal, inpainting, colorization, and scene recomposition.

In summary, 1) we propose a novel approach that leverages semantic correlations between 3D Gaussians for efficient scene editing; 2) We design an efficient training pipeline that shapes the scene representation once and ensures that the perturbed representation continues to support coherent edits without reshaping along the perturbation trajectory; 3) We demonstrate that our MI shaping technique affects only approximately $\sim 7\%$ of all Gaussians during training, while existing scene-editing methods require optimizing the entire set of Gaussians. Despite the lightweightness, our method achieves significant performance gains in tasks such as 3D segmentation, object removal, and inpainting, while substantially reducing computational and memory overhead.

2 Related works

Neural representations for 3D reconstruction Implicit neural representations have recently transformed the field of 3D reconstruction, such as Neural Radiance Fields (NeRF) (Mildenhall et al., 2021) and its extensions (Barron et al., 2022; Deng et al., 2022; Karras et al., 2021; Liu et al., 2020; Martin-Brualla et al., 2021; Zhang et al., 2023), which utilize neural networks to parameterize 3D scenes, enabling detailed and accurate reconstructions. Subsequent advancements have focused on optimizing the NeRF framework for large-scale scenes. Techniques such as multi-resolution hash tables and voxel grids have been proposed to compress scene representations (Garbin et al., 2021; Müller et al., 2022; Reiser et al., 2021). Additionally, hybrid approaches have incorporated explicit modeling strategies, leveraging point clouds to enhance scene representation (Fridovich-Keil et al., 2022; Xu et al., 2022; Kerbl et al., 2023). Notably, 3D Gaussian Splatting (3DGS) (Kerbl et al., 2023) employs point-wise Gaussians to achieve efficient training and rendering. These 3D representations are useful for various downstream tasks, such as semantic understanding (Zhi et al., 2021; Bao et al., 2023; Wang et al., 2023b; Gao et al., 2022; Li et al., 2024), segmentation (Fu et al., 2022; Ye et al., 2023; Cen et al., 2023), and 3D content creation (Tang et al., 2023; Chen et al., 2023b). Nevertheless, current methods predominantly rely on first-order supervision, often neglecting the higher-order correlations encoded in the scene representation.

Scene representations for 3D editing Despite advancements in reconstruction, interactive 3D scene editing remains challenging. Current neural representation-based approaches (Wang et al., 2022; Yuan et al., 2022; Schwarz et al., 2020; Wang et al., 2023a; Zhou et al., 2023; Chen et al., 2023a) typically rely on attributes computed by distilling features from 2D foundation models and perform editing in a point-wise manner. In contrast, our work delves into manipulating scenes based on a second-order correlation structure. The idea of enforcing second-order correlation is first proposed in JacobiNeRF (Xu et al., 2023), while it mainly focuses on label propagation and one-time perturbation consistency, limiting its potential for diverse scene manipulations. Furthermore, the correlation shaping in Xu et al. (2023) is both memory- and time-intensive during the training. Other approaches involve using physics simulators to guide scene editing (Li et al., 2023; Xie et al., 2023), yet incurring a high computational cost in solving partial differential equations at inference time. Our approach offers efficient optimization and enables fast scene editing during inference by learning continuously well-shaped tangent spaces.

3 Modeling mutual information between 3D gaussians

Our goal is to develop scene representations that not only capture 3D geometry and appearance with high precision but also encode the interrelationships between individual elements. These enriched

representations enable efficient scene editing by ensuring coherent and realistic updates, where changes propagate in a coordinated and intuitive manner.

Building on 3D Gaussian Splatting (3DGS) (Kerbl et al., 2023), a state-of-the-art technique for 3D reconstruction that represents scenes using independent sets of 3D Gaussians, we aim to introduce meaningful correlations between these Gaussians. To achieve this, we incorporate mutual information (MI) to capture their underlying interdependence. However, traditional MI-based methods involve heavy optimization processes and are typically applied point-wise, meaning they are valid only for the current representation. This renders them unsuitable for scene editing, which requires both real-time response and persistent editability.

To overcome this limitation, we propose a novel training approach that efficiently shapes the attribute decoding network to capture and maintain these correlations throughout the decoding process. Notably, these structured correlations persist even after multiple consecutive scene edits. Finally, we demonstrate how these well-formed correlations improve a range of downstream scene editing tasks.

3.1 Preliminaries: 3D gaussian splatting and attibute decoding

Given a dataset $\mathcal{D}$ consisting of multi-view 2D images and corresponding camera poses, 3D Gaussian Splatting (3DGS) reconstructs the 3D scene by learning a set of 3D Gaussians $\mathcal{G} = \{\mathbf{g}_1, \mathbf{g}_2, ..., \mathbf{g}_N\}$, where N denotes the number of 3D Gaussians in the entire scene. Each 3D Gaussian $\mathbf{g}_i$ possesses multiple attributes, denoted as $\{\mathbf{x}_i, \mathbf{s}_i, \mathbf{q}_i, \mathbf{o}_i, \mathbf{c}_i\}$. Specifically, $\mathbf{x}_i \in \mathbb{R}^3$ represents the location of the centroid of $\mathbf{g}_i$, $\mathbf{s}_i \in \mathbb{R}^3$ denotes the scale, and $\mathbf{q}_i \in \mathbb{R}^4$ denotes the rotational quaternion, such that $\mathbf{s}_i$ and $\mathbf{q}_i$ jointly represent the 3D covariance matrix $\mathbf{\Sigma}$ of $\mathbf{g}_i$. Additionally, $\mathbf{o}_i \in \mathbb{R}$ represents the opacity, and $\mathbf{c}_i$ denotes the color, which is represented as the spherical harmonics (SH) coefficients. Given a camera pose, the color $C(p)$ of a pixel p can be computed by blending a set of depth-ordered Gaussians $\mathcal{N}$ that overlap with p:

$$C(p) = \sum_{i \in \mathcal{N}} \mathbf{c} i \alpha_i \prod_{j=1}^{i-1} (1 - \alpha_j), \tag{1}$$

where $\mathbf{c}_i$ is the color of the i-th Gaussian, and α_i is the blending weight, calculated using the opacity, projected 2D covariance of the Gaussian, and the location of the pixel.

While 3DGS offers several advantages, its sparse and unorganized structure leads to significant storage demands and makes scalability challenging. To address this, mutual relationships between Gaussians have been explored in subsequent works to eliminate structural redundancies. Lu et al. (2023); Lee et al. (2024) proposed leveraging spatial relationships (i.e., features of Gaussians in a local region tend to have similar values) by employing neural networks to decode their features:

$$a(\mathbf{g}_i) = \mathbf{\Phi}_a(f(\mathbf{g}_i), d; \theta), \tag{2}$$

where $a(\mathbf{g}_i)$ denotes attributes such as the color $\mathbf{c}_i$ of the Gaussian $\mathbf{g}_i$. The Gaussian attributes are decoded by an attribute decoding network $\mathbf{\Phi}_a$ with parameters θ, taking the feature of the Gaussian $f(\mathbf{g}_i)$ and the viewing direction d as inputs. Incorporating the viewing direction into inputs improves the scene representation's robustness to substantial viewpoint changes and lighting effects.

Although associating millions of Gaussians via a network has proven effective, we argue that deeper exploration of the correlation structure of Gaussians through mutual information can further enhance scene editing, enabling better coordination among Gaussians for more effective results.

3.2 Mutual information between 3D gaussians

Traditional 3DGS losses predominantly focus on first-order supervision, optimizing for view synthesis rather than scene interaction. In contrast, this work introduces second-order supervision to shape the attribute decoding multilayer perceptron (MLP), facilitating efficient scene editing. Specifically, we optimize the network parameters to induce a global structure that encodes correlations among individual Gaussians. This ensures that modifications to the attribute decoding network's parameters, denoted by θ, directly correspond to meaningful scene-editing operations. As a result, network outputs produce coherent and semantically consistent editing effects in the rendered scene, driven by the learned co-variation correlations.

To formalize this, we study the correlations between Gaussians under representation parameter changes in the output attributes. We analyze this behavior by considering two randomly selected Gaussians, $\mathbf{g}_i$ and $\mathbf{g}_j$, and their corresponding offsets in output attributes, $\hat{a}(\mathbf{g}_i)$ and $\hat{a}(\mathbf{g}_j)$. These attribute changes arise from the perturbed network $\hat{F}_a(\cdot;\theta^D + \mathbf{n})$, where $\mathbf{n} \in \mathbb{R}^D$ represents a perturbation applied to the parameter set θ^D.

Following Xu et al. (2023), we show that the mutual information between the attribute variations $\hat{a}(\mathbf{g}_i)$ and $\hat{a}(\mathbf{g}_j)$ is proportional to the cosine similarity of the Jacobians of $\mathbf{\Phi}_a$ with respect to the perturbed parameters θ_D:

$$\mathbb{I}(\hat{a}(\mathbf{g}_i), \hat{a}(\mathbf{g}_j)) = \log\left(\frac{1}{\sqrt{1-\cos^2(\gamma)}}\right) + \text{const.}, \tag{3}$$

where γ denotes the angle between the Jacobians $\frac{\partial \mathbf{\Phi}_a(f(\mathbf{g}_i,d);\theta)}{\partial \theta_D}$ and $\frac{\partial \mathbf{\Phi}_a(f(\mathbf{g}_j),d;\theta)}{\partial \theta_D}$. For clarity, we denote the Jacobians as $\partial \mathbf{\Phi}_i$ and $\partial \mathbf{\Phi}_j$. This formulation reveals that the mutual information $\mathbb{I}(\hat{a}(\mathbf{g}_i), \hat{a}(\mathbf{g}_j))$ is positively correlated with the cosine similarity of their gradients with respect to the perturbed parameters.

We apply Eq. 3 to evaluate whether the correlations between Gaussians are well-structured by the attribute decoding network $\mathbf{\Phi}_a$. As shown in Fig. 2 (a), network weights optimized solely by the reconstruction loss fail to reveal meaningful correlations between Gaussians, primarily due to the unstructured nature of 3DGS. Despite the association of millions of Gaussians via the decoding network, they remain disorganized— a limitation of methods optimized solely for novel view synthesis.

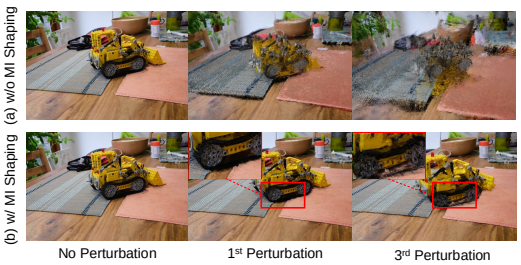

Figure 2: Perturb the attribute decoding network by the Jacobian of a Gaussian in the bulldozer without (a) or with (b) MI shaping (Xu et al., 2023), and then move Gaussians according to similarities of Jacobian with selected one.

JacobiNeRF (Xu et al., 2023) addresses this by enforcing perturbation consistency through maximizing the quantity in Eq. 3, enabling label propagation tasks. However, this approach is not suitable for scene editing in the 3DGS framework for two main reasons: (1) It does not support consecutive scene editing. As shown in Fig. 2 (b), previous MI shaping fails after multiple editing operations, leading to unrealistic scene updates. This is because the shaping in Xu et al. (2023) is *point-wise*: while $\partial \mathbf{\Phi}_i$ and $\partial \mathbf{\Phi}_j$ may be similar in the original tangent space, there is no guarantee that they remain similar after parameter perturbation. (2) The optimization process is complex, requiring substantial storage to maintain the computational graph and significant time for Jacobian computation. This approach is inefficient for 3DGS and fails to meet the real-time demands of user-driven scene interactions.

Next, we will discuss how to ensure consistency across consecutive parameter changes while maintaining training efficiency.

3.3 Mutual Information Shaping with Consistency and Efficiency

To ensure consistency in correlation shaping after perturbation, we begin by formulating the gradient expression for an in-depth analysis. Given that attribute decoding networks in neural fields (e.g., NeRFs and 3DGS) are MLPs, we focus on perturbing the weights $W^{(l)}$ of the l-th linear layer in the network $\mathbf{\Phi}_a$ (i.e., $\theta_D = W^{(l)}$), expressed as $h^{(l)} = W^{(l)}\sigma(h^{(l-1)}) + b^{(l)}$. Here, σ denotes the non-linear activation function, $b^{(l)}$ is the bias, and $h^{(l)}$ is the (hidden) output of the l-th layer.

To reveal the relationship between the gradient of a Gaussian $\mathbf{g}_i$, $\partial \mathbf{\Phi}_i = \frac{\partial \mathbf{\Phi}(f(\mathbf{g}_i,d);\theta)}{\partial \theta_D}$, and the perturbed weight $W^{(l)}$, we consider the gradient of an arbitrary scalar output z in the attribute decoding network with respect to $W^{(l)}$:

$$z = Y(h^{(l)}) = Y(W^{(l)}\sigma(h^{(l-1)}) + b^{(l)}), \tag{4}$$

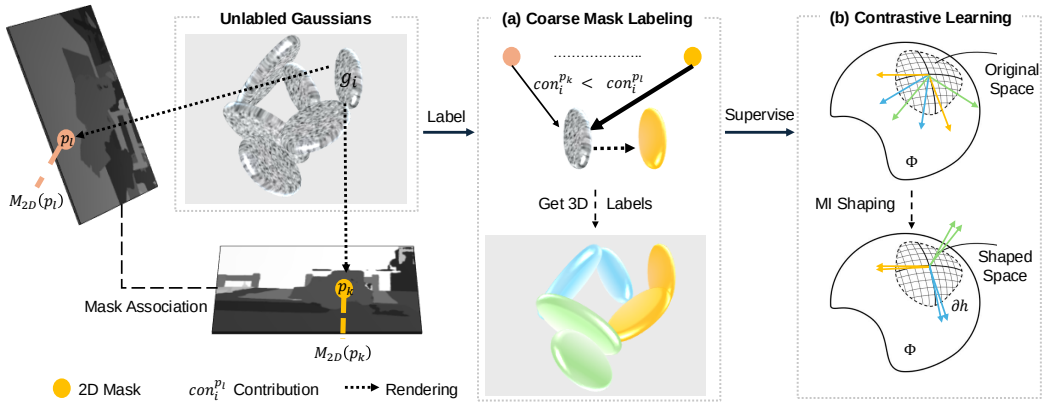

Figure 3: The training pipeline of our correlation shaping: **(a)** We use SAM Kirillov et al. (2023) to generate 2D masks and a pre-trained zero-shot tracker Cheng et al. (2023) to associate masks from different views. We label the 3D mask of each Gaussian according to the 2D mask of the pixel that owns the Gaussian's maximal contribution during rendering across all views. **(b)** We use the labeled 3D masks as the supervision to conduct contrastive learning for mutual information shaping. After shaping, the Jacobians are consistently distributed in the tangent space.

where Y denotes all transformations after the l-th layer, and z is an arbitrary scalar in the vector output of $\mathbf{\Phi}$. The differential $\mathrm{d}z$ can be written as:

$$\mathrm{d}z = \frac{\partial z}{\partial h^{(l)}}^{\top} \mathrm{d}h^{(l)} = \sigma(h^{(l-1)}) \frac{\partial z}{\partial h^{(l)}}^{\top} \mathrm{d}W^{(l)} = \mathrm{tr}(\sigma(h^{(l-1)}) \frac{\partial z}{\partial h^{(l)}}^{\top} \mathrm{d}W^{(l)}), \tag{5}$$

since $\mathrm{d}z = \mathrm{tr}\left(\frac{\partial z}{\partial W^{(l)}}^{\top} \mathrm{d}W^{(l)}\right)$, we can derive:

$$\frac{\partial z}{\partial W^{(l)}} = \frac{\partial z}{\partial h^{(l)}} \sigma(h^{(l-1)})^{\top}. \tag{6}$$

By expressing $\cos(\gamma)$ in Eq. 3 using the right-hand side of Eq. 6, we derive:

$$\cos(\partial \mathbf{\Phi}_i^{(d)}, \partial \mathbf{\Phi}_j^{(d)}) \approx \cos(\partial h_i^{(0)}, \partial h_j^{(0)}), \quad d \in \mathbb{N}, \tag{7}$$

when $\partial h_i^{(0)}$ and $\partial h_j^{(0)}$ point in the same or opposite directions. Here, $\partial \mathbf{\Phi}_i^{(d)}$ represents the Jacobian after the d-th perturbation, and $\partial h_i^{(0)}$ represents the Jacobian $\frac{\partial h^{(l)}}{\partial W^{(l)}}$ of $\mathbf{g}_i$ without perturbation. Upon further derivation, we find that ∂h corresponds to repeated activations $\sigma(h^{(l-1)})$. A detailed derivation and the proof of Eq. 7 can be found in the Appendix C. Eq. 7 indicates that activation shaping can substitute for Jacobian calculation in Eq. 7 to satisfy object-level mutual relations, i.e., $\|\cos(\gamma)\|$ approaches 1 if $\mathbf{g}_i$ and $\mathbf{g}_j$ belong to the same object, or approaches 0 if not.

The key insight of Eq. 7 is that by optimizing activations instead of Jacobians, the correlations between Gaussians can be correctly shaped and remain consistent after successive parameter changes. This enables versatile editing operations in the scene and makes training much more efficient, as there is no need to maintain the computational graph for Jacobian calculation.

3.4 Shaping Correlations Between Gaussians for Scene Editing

According to Eq. 3 and Eq. 7, to ensure that two 3D Gaussians remain highly correlated consistently even after parameter changes – thus supporting a sequence of editing operations without reshaping the parameters – we shape their activations ∂h within the attribute decoding network $\mathbf{\Phi}a$. To enable meaningful scene editing, we define positive and negative pairs based on object-level relationships, where (g_i, g_i^+) represents a pair of Gaussians belonging to the same entity, and (g_i, g_i^-) are independent Gaussians. For positive pairs, we align their activations in $\mathbf{\Phi}a$ relative to the perturbed layer $W^{(l)}$, while for negative pairs with minimal mutual information, we enforce their ∂h to be orthogonal. To achieve this, we minimize the InfoNCE loss (van den Oord et al., 2018):

$$\mathcal{L}_{\text{MI}} = -\log \frac{\exp(|\cos(\partial h_i, \partial h_{i^+})|/\tau)}{\sum_{i^+ \cup \{i^-\}} \exp(|\cos(\partial h_i, \partial h_{i^-})|/\tau)}, \tag{8}$$

where τ is the temperature parameter. This loss encourages highly correlated Gaussians to exhibit large activation similarity while ensuring that uncorrelated Gaussians exhibit near-zero similarity.

3.5 SUPERVISION REFINEMENT

We now address how to sample positive and negative pairs from all 3D Gaussians. Identifying the label of each 3D Gaussian is challenging, as 3DGS is trained from a set of 2D posed images, complicating the recovery of the joint 3D distribution. However, by leveraging the advances of 2D vision foundation models (Kirillov et al., 2023), we label a coarse mask by lifting 2D mask to 3D:

$$M_{3D}(g_i) = M_{2D}(\arg\max_p con_i^p), \tag{9}$$

where con_i^p represents the contribution of g_i to pixel p during rendering, and M_{3D} and M_{2D} denote the 3D mask of Gaussians and the 2D mask of pixels. Eq. 9 indicates that the mask of a 3D Gaussian g_i is determined by the 2D mask of a pixel where g_i contributes the most across all 2D images. We compute the contribution con_i^p based on a trained 3DGS that contains geometric priors of the scene. Thus the mask of g_i is likely to be determined by the 2D mask where its maximal contribution appears. In order to harmonize 2D mask IDs produced from different views, we use a pre-trained zero-shot tracker (Cheng et al., 2023) to associate 2D masks by treating them as a video sequence. We also provide a version without using tracker in the experiments, and it is elaborated in the Appendix.

To further enhance efficiency, we introduce a smoothness regularization in the self-supervised training. Since objects are continuous in space, neighboring Gaussians of $\mathbf{g}i$ are likely to belong to the same object as $\mathbf{g}_i$. This observation helps shape the Jacobians of 3D Gaussians that are heavily occluded by others and may not be accurately annotated in the coarse 3D segmentation. Such Gaussians can be supervised by nearby, well-labeled Gaussians. Specifically, $\mathcal{L}_R$ is formulated as:

$$\mathcal{L}_R = \mathbb{E}_{\mathbb{P}}[\frac{1}{k}\sum_{x^+\in n(x)} 1.0 - \cos(\mathbf{\Phi}_x, \mathbf{\Phi}_{x^+})], \tag{10}$$

where $\mathbb{P}$ denotes the input space, $n(x)$ represents the neighboring Gaussians of x, and $k = \|n(x)\|$ is the number of neighbors. In practice, the distance between two Gaussians is defined by the Euclidean distance between their centroids $\mathbf{x}$, and k is a fixed hyperparameter during training.

3.6 FULL SHAPING PIPELINE

Fig. 3 illustrates our training pipeline, and the total loss as follows:

$$\mathcal{L} = \mathcal{L}_{3DGS} + \lambda_m \mathcal{L}_{MI} + \lambda_r \mathcal{L}_R, \tag{11}$$

where $\mathcal{L}_{3DGS}$ is the photometric reconstruction loss from the original 3DGS pipeline, $\mathcal{L}_{MI}$ is the contrastive learning loss (Eq. 8), and $\mathcal{L}_R$ is the regularization loss, with λ_r representing its corresponding weight.

3.7 CORRELATION-BASED SCENE EDITING

After shaping the correlations, scene editing is performed by perturbing the parameters of the attribute decoding network. Specifically, we perturb the attribute decoding network by applying the average Jacobian $\partial\mathbf{\Phi}_a$ of user-selected Gaussians. When editing through a 2D image rather than directly in 3D space, we select the Gaussians that have the largest influence on the color of the user-selected pixels, similar to the contribution calculation in Eq. 9.

Different branches of the network produce distinct editing effects. For object removal, we perturb the opacity branch $\mathbf{\Phi}_o$ in the gradient direction that reduces output opacity. This can drive the opacity of the relevant Gaussians to zero, effectively removing the object in the rendered scene. For object re-colorization, we perturb the color branch $\mathbf{\Phi}_c$ along different gradient directions of output channels to generate diverse color changes. In the case of 3D segmentation and object movement, we move Gaussians according to similarities in Jacobian with the selected one. When extending to dynamic scenes (Pumarola et al., 2020), we achieve object movement by shaping and perturbing the motion network. Additional editing tasks are discussed in the Appendix.

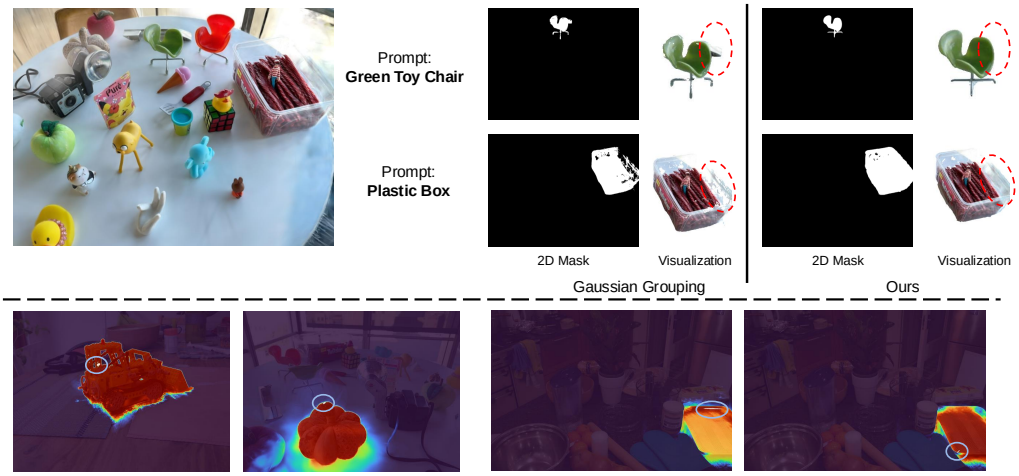

Figure 4: Top: qualitative results of open vocabulary segmentation Ye et al. (2023). Bottom: gallery of relevance maps when perturbing a single Gaussian (highlighted in the purple circle).

4 Experiments

4.1 Implementation Details

Training. We shape mutual information between Gaussians starting from a pre-trained 3D Gaussian Splatting, applying a fine-tuning stage for optimizing attribute decoding network $\mathbf{\Phi}_a$. We follow the shaping pipeline in Fig. 3 for 1500 iterations. The finetuning stage is conducted on a single RTX 3090 GPU for about 1 minute. Detailed hyper-parameter settings can be found in the Appendix.

Datasets. We test our method on open-world datasets LERF-Localization (Kerr et al., 2023), derived LERF-Mask dataset (Ye et al., 2023) with ground-truth segmentation, and Mip-NeRF 360 (Barron et al., 2022), in order to evaluate the segmentation and editing quality in complex and compositional scenarios. We also test the effectiveness of our shaping on the real dynamic scenes in the D-NeRF dataset (Pumarola et al., 2021). Additionally, we provide results on the outdoor unbounded scenes in dataset NERDS 360 (Irshad et al., 2023) in the Appendix.

4.2 3D Segmentation

After shaping the correlations among Gaussians, our approach enables 3D segmentation by simply perturbing the network parameters. We use Grounding DINO (Liu et al., 2023) to generate the 2D mask prompt. We compare our method with the state-of-the-art open vocabulary 3D segmentation methods, including both the NeRF-based (Kerr et al., 2023; Cen et al., 2023), and 3DGS-based methods (Xu et al., 2023; Ye et al., 2023). It's worth noting that Gaussian Grouping (Ye et al., 2023) use the consistent 2D masks generated from the video tracker. To evaluate the effectiveness of our improvement on correlation shaping, we utilize the MI shaping loss in JacobiNeRF (Xu et al., 2023) as a substitute for our MI shaping $\mathcal{L}_{MI}$ in Eq. 11, which only permits one-time perturbation consistency. While keeping other loss terms and supervision refinement the same for a fair comparison, we name the baseline *JaocbiGS*. We also include the results of using foundation models.

For quantitative results, Tab. 1 demonstrates that ours significantly outperforms than both NeRF-based and GS-based methods. Compared with previous state-of-the-art results, our method increases the mIoU by averagely 11%. Qualitative results are shown in Fig. 4. We can see that our method produces sharp boundaries for the segmentation without less blurs. We also provide the relevance map when perturbing a single Gaussian to select the object. The relevance scores are represented as the cosine similarities of the Jacobians $\partial\mathbf{\Phi}$ of the perturbed Gaussian and all other Gaussians. As in Fig. 4, when perturbing a single Gaussian, the corresponding object is highlighted, evidencing ours capability of segmentation from another viewpoint. It also shows that the relevance of Jacobian would be higher if a Gaussian is closer to the perturbed one. These phenomena comply with our expectations, indicating the effectiveness of the proposed MI shaping.

Table 1: Quantitative results of Open Vocabulary Segmentation on LERF-Mask dataset. The time and memory costs mentioned refer to the total consumption of training and finetuning (if have). Comparisons with non-3DGS method in this table are not feasible.

Model	figurines		ramen		teatime		Average Training Cost		
	mIoU	mBIoU	mIoU	mBIoU	mIoU	mBIoU	Time/Minutes	Memory/M	#GS Used
JacobiNeRF (Xu et al., 2023)	22.4	27.6	7.2	6.9	42.6	36.9	*	*	*
LERF (Kerr et al., 2023)	33.5	30.6	28.3	14.7	49.7	42.6	*	*	*
DEVA (Cheng et al., 2023)	46.2	45.1	56.8	51.1	54.3	52.2	*	*	*
SA3D (Cen et al., 2023)	24.9	23.8	7.4	7.0	42.5	39.2	*	*	*
JacobiGS Xu et al. (2023)	62.2	60.1	64.3	57.7	69.7	70.1	30.2	160.2	17%
Gaussian Grouping Ye et al. (2023)	69.7	67.9	77.0	68.7	71.7	66.1	55.2	757.2	100%
Ours w/o DEVA & Regularization	72.2	69.8	79.5	69.9	77.2	70.1	19.7	160.2	15%
Ours w/o DEVA	72.5	70.3	79.1	69.9	77.8	70.2	19.7	160.2	15%
Ours	**80.6**	**77.2**	**80.6**	**70.1**	**84.5**	**78.7**	**16.3**	**160.2**	**7%**

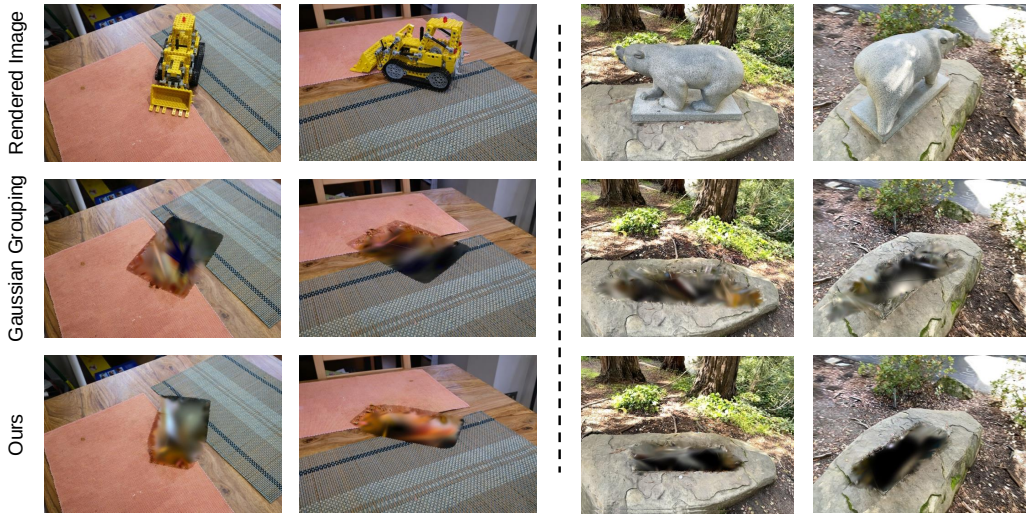

Figure 5: 3D object removal on bear & kitchen scenes. Compared to Gaussian Grouping, our method removes the object with a more fitting curve and less distortion of the irrelevant area.

The superior performance of our methods can be attributed to the learned awareness of the scene structure. Instead of directly assigning scene attributes to each Gaussian Cen et al. (2023); Zhou et al. (2023); Ye et al. (2023), we focus on shaping networks that act on the Gaussians in a way respecting the underlying structures. It helps a lot for the low-level representation like 3DGS when leveraged for the interactive tasks like segmentation and editting. The shaped MLP is aware of the entire scene structure rather than individual Gaussians. Notably, we only sample about 7% of all the Gaussians during finetuning until convergence, boosting the training time while with little memory storage.

4.3 Scene Editing

3D Object removal. 3D object removal is to delete the target object without affecting the background or unrelated area. The space behind the target is unknown from training views and thus it would be noisy after deletion. According to Fig. 5, our method preserves more details of the unrelated area, and the contour of the area caused by the deletion fits the target object shape better. More explicitly, the noisy area resulted from our method after removal in the bear scene accurately matches the rectangle shape of the pedestal of the bear statue. While both are supervised by SAM and DEVA, our method separates the large object more clearly compared to Gaussian Grouping.

3D Object movement. We adopt the task of object movement to evaluate the editing quality under consecutive perturbations. A single perturbation is to add the multiplication of the Jacobian $\partial \mathbf{\Phi}_i$ of selected Gaussian g_i and a scaling factor σ_s for controlling the impact. As shown in Fig. 6, perturbing scenes with the same Gaussian reveals that our method induces reasonable motion (e.g., the carton is lifted up) while preserving the uncorrelated objects. It exhibits path-consistent motion after consecutive perturbations. In contrast, scenes generated by JacobiGS diverge into unrealistic

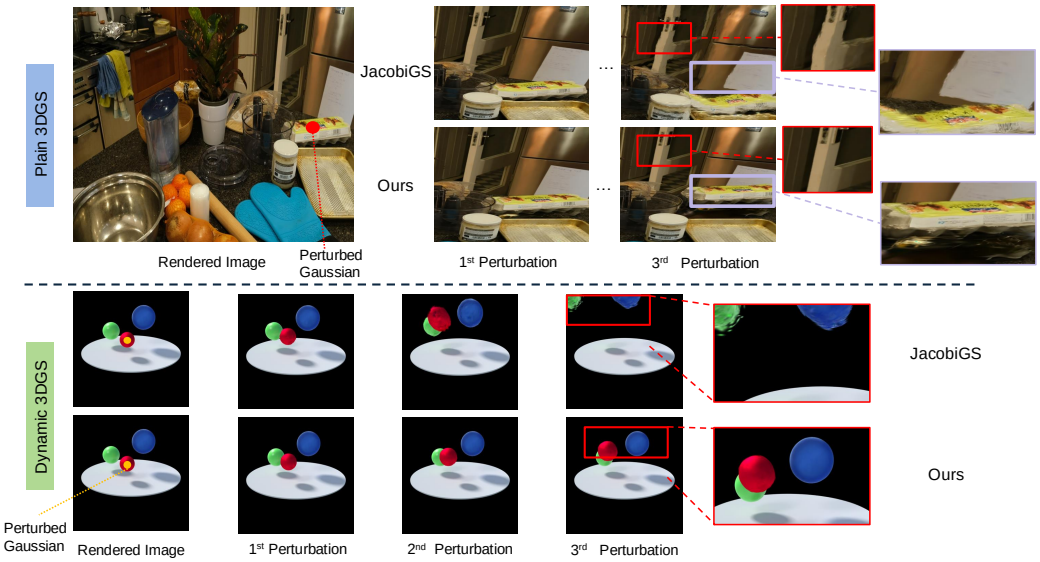

Figure 6: 3D object movement on Mip-NeRF 360 (Barron et al., 2022) and D-NeRF (Pumarola et al., 2020). Compared to the correlation shaping in Xu et al. (2023), our method enables consecutive editing (no need for reshaping) on both static and dynamic scenes, while maintaining consistencies.

Table 2: Ablation study of correlation shaping.

Model	Mip-NeRF 360			D-NeRF		
	PSNR↑	SSIM↑	LPIPS↓	PSNR↑	SSIM↑	LPIPS↓
GS Baseline (Kerbl et al., 2023; Yang et al., 2023)	28.69	0.870	0.182	41.0	0.995	0.009
Ours	28.72	0.842	0.208	39.7	0.993	0.012

representations after the second and third perturbation. For example, consecutive perturbations to the carton result in the distortion of the door behind the box (see the red boxes for highlights in Fig. 6). The observations demonstrate that our method supports continuous editing with consistency, thereby verifying the effectiveness of the proposed shaping technique.

4.4 The effect on the reconstruction quality

We conduct an ablation on how the correlation shaping affects the reconstruction quality. From Tab. 2, we can see that our framework has comparable performance to the baseline method on both static and dynamic scenes. There is a small PSNR drop on dynamics scenes, as we simply integrate our shaping loss into the original deformation network in Yang et al. (2023), which aims for 4D reconstruction, making it a bit challenging to shape all timesteps, and this is subject to future study.

5 Discussion

We attempt the challenge of shaping correlations between independent scene elements in a 3D Gaussian Scene (3DGS) model to enable scene editing through network parameter perturbations. Our derivation demonstrates that enforcing gradient alignment within the network ensures the consistency of mutual information between Gaussians, even after successive parameter perturbations. To achieve this, we introduce an efficient training pipeline, incorporating a contrastive loss and a 2D-to-3D sampling strategy. With the well-shaped correlation structure, we illustrate how the resonance between Gaussians facilitates 3D segmentation and automatically directs millions of Gaussians to respond appropriately to accomplish diverse editing tasks. Despite this efficiency, our current pipeline has limitations when generating arbitrarily complex edits, particularly at a fine-grained level, such as object deformation. In future work, we aim to address this limitation by learning intrinsic object features and kinematics from large-scale video datasets, which would enhance the its capabilities in more sophisticated scene manipulation tasks.

6 REPRODUCIBILITY STATEMENT

We have made significant efforts to ensure the reproducibility of our work. A code example is provided as supplementary material, demonstrating the core components of our approach. Upon acceptance, we will release all of the data and the complete training and testing code to facilitate the full reproducibility of our results.

REFERENCES

Chong Bao, Yinda Zhang, Bangbang Yang, Tianxing Fan, Zesong Yang, Hujun Bao, Guofeng Zhang, and Zhaopeng Cui. Sine: Semantic-driven image-based nerf editing with prior-guided editing field. *2023 IEEE/CVF Conference on Computer Vision and Pattern Recognition (CVPR)*, pp. 20919–20929, 2023. URL https://api.semanticscholar.org/CorpusID:257687450.

Jonathan T Barron, Ben Mildenhall, Dor Verbin, Pratul P Srinivasan, and Peter Hedman. Mip-nerf 360: Unbounded anti-aliased neural radiance fields. In *Proceedings of the IEEE/CVF Conference on Computer Vision and Pattern Recognition*, pp. 5470–5479, 2022.

Richard Bronson. Matrix methods: An introduction. 1969. URL https://api.semanticscholar.org/CorpusID:117111125.

Tim Brooks, Aleksander Holynski, and Alexei A Efros. Instructpix2pix: Learning to follow image editing instructions. In *Proceedings of the IEEE/CVF Conference on Computer Vision and Pattern Recognition*, pp. 18392–18402, 2023.

Jiazhong Cen, Zanwei Zhou, Jiemin Fang, Wei Shen, Lingxi Xie, Dongsheng Jiang, Xiaopeng Zhang, Qi Tian, et al. Segment anything in 3d with nerfs. *Advances in Neural Information Processing Systems*, 36:25971–25990, 2023.

Yihang Chen, Qianyi Wu, Jianfei Cai, Mehrtash Harandi, and Weiyao Lin. Hac: Hash-grid assisted context for 3d gaussian splatting compression. *ArXiv*, abs/2403.14530, 2024. URL https://api.semanticscholar.org/CorpusID:268553921.

Yiwen Chen, Zilong Chen, Chi Zhang, Feng Wang, Xiaofeng Yang, Yikai Wang, Zhongang Cai, Lei Yang, Huaping Liu, and Guosheng Lin. Gaussianeditor: Swift and controllable 3d editing with gaussian splatting. *ArXiv*, abs/2311.14521, 2023a. URL https://api.semanticscholar.org/CorpusID:265445359.

Zilong Chen, Feng Wang, and Huaping Liu. Text-to-3d using gaussian splatting. *ArXiv*, abs/2309.16585, 2023b. URL https://api.semanticscholar.org/CorpusID:263139613.

Ho Kei Cheng, Seoung Wug Oh, Brian Price, Alexander Schwing, and Joon-Young Lee. Tracking anything with decoupled video segmentation. In *ICCV*, 2023.

Kangle Deng, Andrew Liu, Jun-Yan Zhu, and Deva Ramanan. Depth-supervised nerf: Fewer views and faster training for free. In *Proceedings of the IEEE/CVF Conference on Computer Vision and Pattern Recognition*, pp. 12882–12891, 2022.

Zhiwen Fan, Kevin Wang, Kairun Wen, Zehao Zhu, Dejia Xu, and Zhangyang Wang. Lightgaussian: Unbounded 3d gaussian compression with 15x reduction and 200+ fps. *ArXiv*, abs/2311.17245, 2023. URL https://api.semanticscholar.org/CorpusID:265498655.

Sara Fridovich-Keil, Alex Yu, Matthew Tancik, Qinhong Chen, Benjamin Recht, and Angjoo Kanazawa. Plenoxels: Radiance fields without neural networks. In *Proceedings of the IEEE/CVF Conference on Computer Vision and Pattern Recognition*, pp. 5501–5510, 2022.

Xiao Fu, Shangzhan Zhang, Tianrun Chen, Yichong Lu, Lanyun Zhu, Xiaowei Zhou, Andreas Geiger, and Yiyi Liao. Panoptic nerf: 3d-to-2d label transfer for panoptic urban scene segmentation. In *2022 International Conference on 3D Vision (3DV)*, pp. 1–11. IEEE, 2022.

Xuan Gao, Chenglai Zhong, Jun Xiang, Yang Hong, Yudong Guo, and Juyong Zhang. Reconstructing personalized semantic facial nerf models from monocular video. *ACM Transactions on Graphics (TOG)*, 41:1 – 12, 2022. URL https://api.semanticscholar.org/CorpusID:252846034.

Stephan J Garbin, Marek Kowalski, Matthew Johnson, Jamie Shotton, and Julien Valentin. Fastnerf: High-fidelity neural rendering at 200fps. In *Proceedings of the IEEE/CVF International Conference on Computer Vision*, pp. 14346–14355, 2021.

Muhammad Zubair Irshad, Sergey Zakharov, Katherine Liu, Vitor Guizilini, Thomas Kollar, Adrien Gaidon, Zsolt Kira, and Rares Ambrus. Neo 360: Neural fields for sparse view synthesis of outdoor scenes. In *Proceedings of the IEEE/CVF International Conference on Computer Vision*, pp. 9187–9198, 2023.

Tero Karras, Miika Aittala, Samuli Laine, Erik Härkönen, Janne Hellsten, Jaakko Lehtinen, and Timo Aila. Alias-free generative adversarial networks. *Advances in neural information processing systems*, 34:852–863, 2021.

Bernhard Kerbl, Georgios Kopanas, Thomas Leimkühler, and George Drettakis. 3d gaussian splatting for real-time radiance field rendering. *ACM Transactions on Graphics*, 42(4), 2023.

Justin Kerr, Chung Min Kim, Ken Goldberg, Angjoo Kanazawa, and Matthew Tancik. Lerf: Language embedded radiance fields. In *International Conference on Computer Vision (ICCV)*, 2023.

Diederik P Kingma and Jimmy Ba. Adam: A method for stochastic optimization. *arXiv preprint arXiv:1412.6980*, 2014.

Alexander Kirillov, Eric Mintun, Nikhila Ravi, Hanzi Mao, Chloe Rolland, Laura Gustafson, Tete Xiao, Spencer Whitehead, Alexander C. Berg, Wan-Yen Lo, Piotr Dollár, and Ross Girshick. Segment anything. *arXiv:2304.02643*, 2023.

Joo Chan Lee, Daniel Rho, Xiangyu Sun, Jong Hwan Ko, and Eunbyung Park. Compact 3d gaussian representation for radiance field. In *Proceedings of the IEEE/CVF Conference on Computer Vision and Pattern Recognition*, pp. 21719–21728, 2024.

Mingrui Li, Shuhong Liu, and Heng Zhou. Sgs-slam: Semantic gaussian splatting for neural dense slam. *ArXiv*, abs/2402.03246, 2024. URL https://api.semanticscholar.org/CorpusID:267412978.

Xuan Li, Yi-Ling Qiao, Peter Yichen Chen, Krishna Murthy Jatavallabhula, Ming Lin, Chenfanfu Jiang, and Chuang Gan. Pac-nerf: Physics augmented continuum neural radiance fields for geometry-agnostic system identification. *ArXiv*, abs/2303.05512, 2023. URL https://api.semanticscholar.org/CorpusID:257427479.

Lingjie Liu, Jiatao Gu, Kyaw Zaw Lin, Tat-Seng Chua, and Christian Theobalt. Neural sparse voxel fields. *Advances in Neural Information Processing Systems*, 33:15651–15663, 2020.

Shilong Liu, Zhaoyang Zeng, Tianhe Ren, Feng Li, Hao Zhang, Jie Yang, Chunyuan Li, Jianwei Yang, Hang Su, Jun Zhu, et al. Grounding dino: Marrying dino with grounded pre-training for open-set object detection. *arXiv preprint arXiv:2303.05499*, 2023.

Tao Lu, Mulin Yu, Linning Xu, Yuanbo Xiangli, Limin Wang, Dahua Lin, and Bo Dai. Scaffold-gs: Structured 3d gaussians for view-adaptive rendering. *ArXiv*, abs/2312.00109, 2023. URL https://api.semanticscholar.org/CorpusID:265551778.

Ricardo Martin-Brualla, Noha Radwan, Mehdi SM Sajjadi, Jonathan T Barron, Alexey Dosovitskiy, and Daniel Duckworth. Nerf in the wild: Neural radiance fields for unconstrained photo collections. In *Proceedings of the IEEE/CVF Conference on Computer Vision and Pattern Recognition*, pp. 7210–7219, 2021.

Ben Mildenhall, Pratul P Srinivasan, Matthew Tancik, Jonathan T Barron, Ravi Ramamoorthi, and Ren Ng. Nerf: Representing scenes as neural radiance fields for view synthesis. *Communications of the ACM*, 65(1):99–106, 2021.

Thomas Müller, Alex Evans, Christoph Schied, and Alexander Keller. Instant neural graphics primitives with a multiresolution hash encoding. *ACM Transactions on Graphics (ToG)*, 41(4): 1–15, 2022.

Onur Özyeşil, Vladislav Voroninski, Ronen Basri, and Amit Singer. A survey of structure from motion*. *Acta Numerica*, 26:305–364, 2017.

Albert Pumarola, Enric Corona, Gerard Pons-Moll, and Francesc Moreno-Noguer. D-nerf: Neural radiance fields for dynamic scenes. *2021 IEEE/CVF Conference on Computer Vision and Pattern Recognition (CVPR)*, pp. 10313–10322, 2020. URL https://api.semanticscholar.org/CorpusID:227227965.

Albert Pumarola, Enric Corona, Gerard Pons-Moll, and Francesc Moreno-Noguer. D-nerf: Neural radiance fields for dynamic scenes. In *Proceedings of the IEEE/CVF Conference on Computer Vision and Pattern Recognition*, pp. 10318–10327, 2021.

Christian Reiser, Songyou Peng, Yiyi Liao, and Andreas Geiger. Kilonerf: Speeding up neural radiance fields with thousands of tiny mlps. *2021 IEEE/CVF International Conference on Computer Vision (ICCV)*, pp. 14315–14325, 2021. URL https://api.semanticscholar.org/CorpusID:232352619.

Katja Schwarz, Yiyi Liao, Michael Niemeyer, and Andreas Geiger. Graf: Generative radiance fields for 3d-aware image synthesis. *Advances in Neural Information Processing Systems*, 33: 20154–20166, 2020.

Roman Suvorov, Elizaveta Logacheva, Anton Mashikhin, Anastasia Remizova, Arsenii Ashukha, Aleksei Silvestrov, Naejin Kong, Harshith Goka, Kiwoong Park, and Victor Lempitsky. Resolution-robust large mask inpainting with fourier convolutions. In *Proceedings of the IEEE/CVF winter conference on applications of computer vision*, pp. 2149–2159, 2022.

Jiaxiang Tang, Jiawei Ren, Hang Zhou, Ziwei Liu, and Gang Zeng. Dreamgaussian: Generative gaussian splatting for efficient 3d content creation. *arXiv preprint arXiv:2309.16653*, 2023.

Zachary Teed and Jia Deng. Raft: Recurrent all-pairs field transforms for optical flow. In *Computer Vision–ECCV 2020: 16th European Conference, Glasgow, UK, August 23–28, 2020, Proceedings, Part II 16*, pp. 402–419. Springer, 2020.

Cyrus Vachha and Ayaan Haque. Instruct-gs2gs: Editing 3d gaussian splats with instructions, 2024. URL https://instruct-gs2gs.github.io/.

Aäron van den Oord, Yazhe Li, and Oriol Vinyals. Representation learning with contrastive predictive coding. *ArXiv*, abs/1807.03748, 2018. URL https://api.semanticscholar.org/CorpusID:49670925.

Binglun Wang, Niladri Shekhar Dutt, and Niloy Jyoti Mitra. Proteusnerf: Fast lightweight nerf editing using 3d-aware image context. *ArXiv*, abs/2310.09965, 2023a. URL https://api.semanticscholar.org/CorpusID:264146680.

Can Wang, Menglei Chai, Mingming He, Dongdong Chen, and Jing Liao. Clip-nerf: Text-and-image driven manipulation of neural radiance fields. In *Proceedings of the IEEE/CVF Conference on Computer Vision and Pattern Recognition*, pp. 3835–3844, 2022.

Ruibo Wang, Song Zhang, Ping Huang, Donghai Zhang, and Wei Yan. Semantic is enough: Only semantic information for nerf reconstruction. *2023 IEEE International Conference on Unmanned Systems (ICUS)*, pp. 906–912, 2023b. URL https://api.semanticscholar.org/CorpusID:265354446.

Tianyi Xie, Zeshun Zong, Yuxin Qiu, Xuan Li, Yutao Feng, Yin Yang, and Chenfanfu Jiang. Physgaussian: Physics-integrated 3d gaussians for generative dynamics. *arXiv preprint arXiv:2311.12198*, 2023.

Qiangeng Xu, Zexiang Xu, Julien Philip, Sai Bi, Zhixin Shu, Kalyan Sunkavalli, and Ulrich Neumann. Point-nerf: Point-based neural radiance fields. In *Proceedings of the IEEE/CVF Conference on Computer Vision and Pattern Recognition*, pp. 5438–5448, 2022.

Xiaomeng Xu, Yanchao Yang, Kaichun Mo, Boxiao Pan, Li Yi, and Leonidas Guibas. Jacobinerf: Nerf shaping with mutual information gradients. In *Proceedings of the IEEE/CVF Conference on Computer Vision and Pattern Recognition (CVPR)*, pp. 16498–16507, June 2023.

Ziyi Yang, Xinyu Gao, Wen Zhou, Shaohui Jiao, Yuqing Zhang, and Xiaogang Jin. Deformable 3d gaussians for high-fidelity monocular dynamic scene reconstruction. *arXiv preprint arXiv:2309.13101*, 2023.

Mingqiao Ye, Martin Danelljan, Fisher Yu, and Lei Ke. Gaussian grouping: Segment and edit anything in 3d scenes. *arXiv preprint arXiv:2312.00732*, 2023.

Yu-Jie Yuan, Yang-Tian Sun, Yu-Kun Lai, Yuewen Ma, Rongfei Jia, and Lin Gao. Nerf-editing: Geometry editing of neural radiance fields. *2022 IEEE/CVF Conference on Computer Vision and Pattern Recognition (CVPR)*, pp. 18332–18343, 2022. URL `https://api.semanticscholar.org/CorpusID:248665648`.

Xiaoshuai Zhang, Abhijit Kundu, Thomas Funkhouser, Leonidas Guibas, Hao Su, and Kyle Genova. Nerflets: Local radiance fields for efficient structure-aware 3d scene representation from 2d supervision. In *Proceedings of the IEEE/CVF Conference on Computer Vision and Pattern Recognition*, pp. 8274–8284, 2023.

Shuaifeng Zhi, Tristan Laidlow, Stefan Leutenegger, and Andrew J Davison. In-place scene labelling and understanding with implicit scene representation. In *Proceedings of the IEEE/CVF International Conference on Computer Vision*, pp. 15838–15847, 2021.

Shijie Zhou, Haoran Chang, Sicheng Jiang, Zhiwen Fan, Zehao Zhu, Dejia Xu, Pradyumna Chari, Suya You, Zhangyang Wang, and Achuta Kadambi. Feature 3dgs: Supercharging 3d gaussian splatting to enable distilled feature fields. *arXiv preprint arXiv:2312.03203*, 2023.

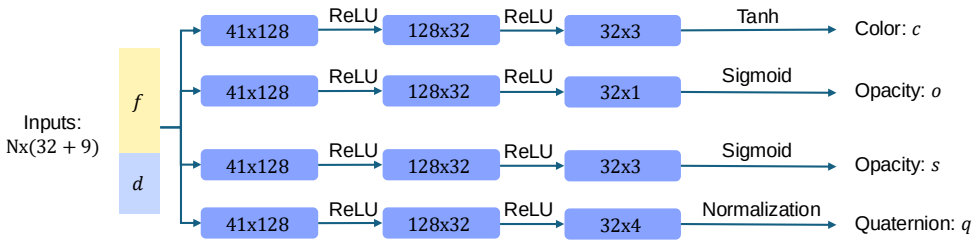

Figure 7: The structure of attribute decoding network. For each 3D Gaussian, we use different branches to predict attributes (opacity, color, scale, and quaternion). The inputs are features of Gaussians with view direction.

A Implementation Details

attribute decoding network. The attribute decoding network is composed of four different branches, including the color branch $\mathbf{\Phi}_c$, opacity branch $\mathbf{\Phi}_o$, and branches for the covariance $\mathbf{\Phi}_s$ and $\mathbf{\Phi}_q$. They are all implemented by MLPs with RELU activation. The detailed structure is illustrated in Fig. 7, where the output activation of different branches is inspired from Lu et al. (2023). The centroid x of each Gaussian is initialized by the pre-computed point cloud from SfM points (Özyeşil et al., 2017) and separately optimized. The hidden dimension of each feature is 32 and initialized to be zero.

Training hyperparamters. During training, we set the hyperparameters $\lambda_{MI} = 0.1$, $\lambda_R = 0.1$ and $k = 5$. We adopt the Adam optimizer Kingma & Ba (2014) when shaping the attribute decoding network, with a learning rate of 0.01. The gradient that we use to shape the motion network is $\partial h = \frac{\partial h^{(l)}}{\partial W^{(l)}}$ of each branch by default, where l is the linear layer before the final output layer. We train the network for 1500 iterations, sampling a random view and a batch of 512 3D Gaussians at each iteration to compute the training loss.

When training in the style of previous mutual information shaping in JacobiNeRF (Xu et al., 2023) to produce the results of JacobiGS, we modify the sampling batch size from 512 to 48 due to the large memory consumption. This is because the shaping method in JacobiNeRF requires the direct calculation of Jacobians $\partial\mathbf{\Phi}$, which necessitates the preservation of the entire computation graph.

Training without using the tracker for mask association. We use DEVA (Cheng et al., 2023) to associate the masks produced from SAM (Kirillov et al., 2023) for training. However, the assumption of using the tracker to associate masks from different views is that the multi-view training images could be treated as a video. It will not hold when training views are sparse and random. In light of this, we introduce another shaping version without mask association, which is supervised by projecting the Jacobians to 2D for a sampled view:

$$\partial\mathbf{\Phi}(p) = \sum_{i\in\mathcal{N}} \partial\mathbf{\Phi}_i \alpha_i \prod_{j=1}^{i-1}(1-\alpha_j), \tag{12}$$

where $\partial\mathbf{\Phi}_i$ is the Jacobian of the i-th Gaussian and α_i is the blending weight that is calculated with the opacity, projected 2D covariance of the Gaussian, and the location of the pixel. By projecting the Jacobians of 3D Gaussians to 2D space, we can now sample Jacobians of pixels instead of 3D Gaussians for contrastive learning. We sample a random view and 512 pixels of it for each iteration, supervised by the 2D mask of this view which is generated from SAM. We keep all other hyperparameters the same as the version of mask association. Note that we still use ∂h to replace $\partial\mathbf{\Phi}$ for Jacobian shaping according to Eq. 7.

Speed-up module. For the MI shaping version without mask association, it would be time-consuming when projecting Jacobians to the 2D plane as the dimension of the Jacobian is high. We then propose a speed-up module that modifies the rasterization process in the CUDA pipeline. As we only need to sample a small batch of Jacobians of pixels at each iteration, we add a mask during the CUDA forward and backward process to avoid the calculation of non-sampled pixels for Jacobians projection.

Figure 8: 3D object Inpainting of our method. We use LAMA (Suvorov et al., 2022) to inpaint the images after object removal, and then finetune Gaussians based on the inpainted 2D images.

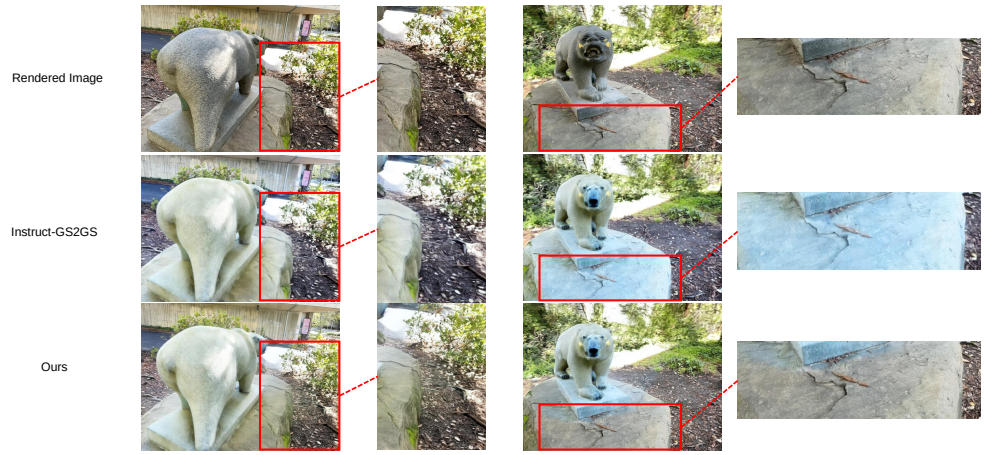

Figure 9: 3D object style transfer. We use Instruct-Pix2Pix (Brooks et al., 2023) to edit the 2D images (prompt: *"Turn the bear into a polar bear"*), and then finetune Gaussians based on the edited 2D images. We compare our method with Instruct-GS2GS (Vachha & Haque, 2024), which is also a 3DGS-based style transfer method.

B Additional Experimental Results

B.1 Scene Editing

3D object inpainting. Based on the 3D object removal, we could further accomplish the task of inpainting. Inspired by Gaussian Grouping (Ye et al., 2023), we first detect the noisy area after object removal through the mask association by DEVA (Cheng et al., 2023), and then use LAMA (Suvorov et al., 2022) to inpaint the noisy deletion area for each view. Finally, we finetune Gaussians with similar training process according to the 2D inpainted images for about 5 minutes to get the 3D inpainting results. Fig. 8 demonstrates the effectiveness of our method for 3D object inpainting.

3D object style transfer. By selecting an object (similar to object removal), we could also achieve 3D object style transfer. First, we select all correlated Gaussians of the object through 3D segmentation. Second, we freeze the parameters of other Gaussians and start finetuning. During finetuning, we use the edited 2D ground truth images as supervision which are produced by Instruct-Pix2Pix (Brooks et al., 2023), updating the original dataset. The pipeline is the same as Instruct-GS2GS. During finetuning, We employ L1 loss inside the 2D mask of the selected object and LPIPS loss within the bounding box that encloses the mask. From Fig. 9, we could see that our method significantly reduced the influence of the area that is not related to the targeted object. Instruct-GS2GS changes the hue of the whole figure and produce artifacts after editing.

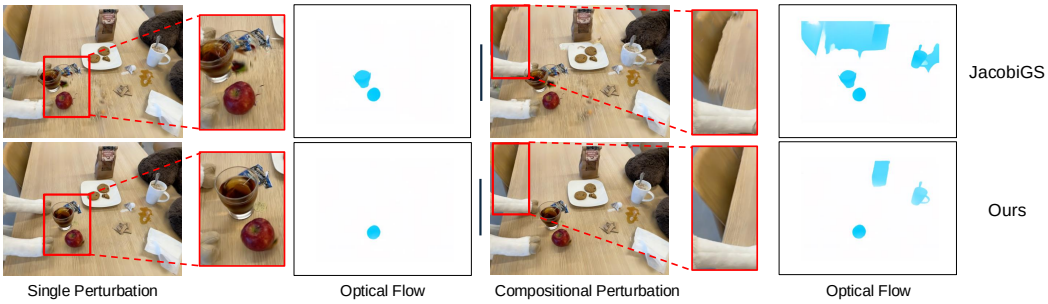

Figure 10: Visual comparison of multi-object editing between JacobiGS (Xu et al., 2023) and ours, where we slightly perturb three different objects: apple, cup, and bag. We use RAFT (Teed & Deng, 2020) to estimate the optical flow for visualizing the movement.

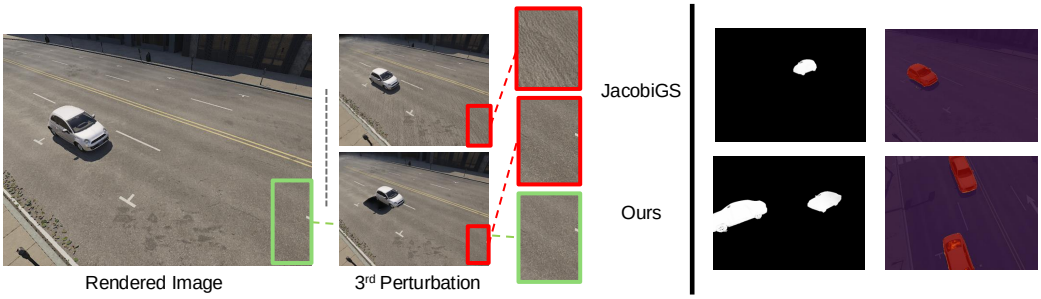

Figure 11: Qualitative results on NeRDS 360 (Irshad et al., 2023). Left: Comparison of consecutive editions when moving the car. Right: The gallery of segmentation mask and relevance map from different views(when perturbing a single Gaussian), obtained by our method.

Multi-object editing. To achieve edit multiple objects in the same scene, we simply add Jacobians of selected Gaussians of different objects to the network parameters. As shown in Fig. 10, JacobiGS has difficulty maintaining scene integrity when combining Jacobians of two or more objects for perturbations. For instance, the table nearby is also affected by the perturbation (see the red box comparison of the right part in Fig. 10). Conversely, our method effectively maintains robust correlation shaping, demonstrating superior performance in preserving the scene under multi-object editing.

B.2 Outdoor Scenarios

To test the generalizability of our method, we employ our shaping method in NeRDS 360 (Irshad et al., 2023), which is an outdoor unbounded dataset comprising 75 unbounded and diverse scenes. From Fig. 11(a), we can clearly see that our method moves the car without creating any artifacts. JacobiGS fails to make the car move while changing the texture of the surrounding road. Fig. 11(b) illustrated the ability to detect objects like cars in the 3D space, showing the potential of our method to be applied in practical scenarios.

B.3 Ablation Studies

Robustness of correlation shaping. Though the masks generated by SAM (Kirillov et al., 2023) with DEVA (Cheng et al., 2023) are associated from different views, this strategy still suffers from the multi-granularity across different views and 2D segmentation errors. Fig. 12 demonstrates that our method resolves these problems by shaping the correlations between 3D Gaussians. Given a small part of the object as the prompt, our method can produce the segmentation of the entire object, showing that Gaussians inside the object are greatly associated.

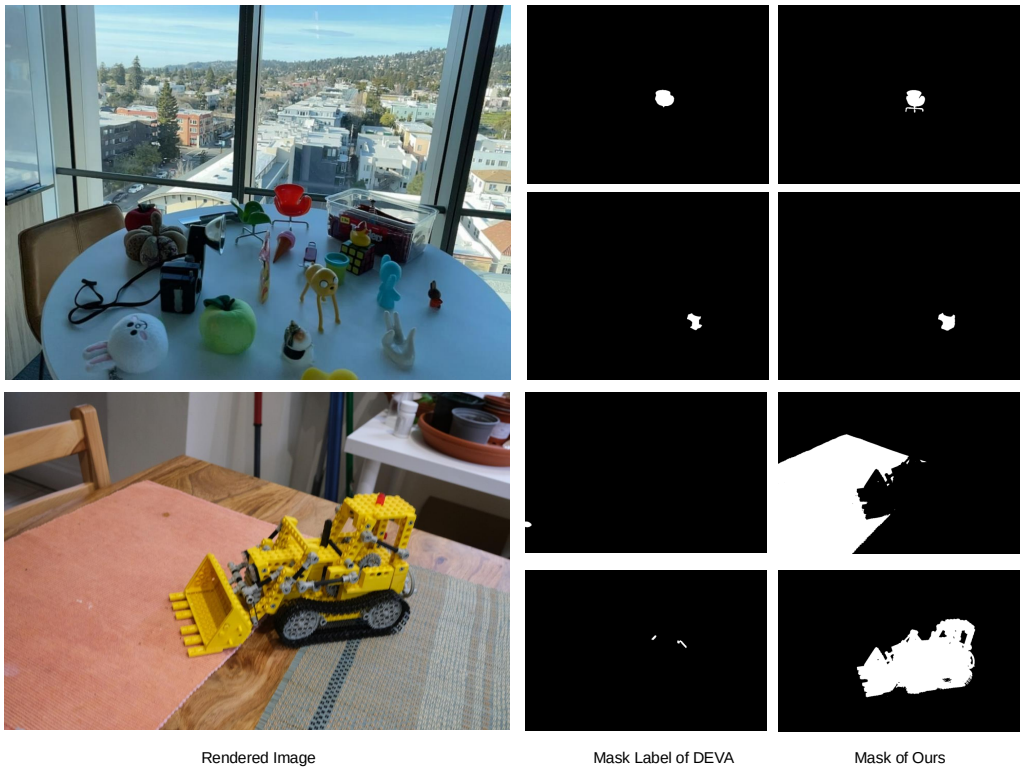

Figure 12: Robustness of our method to the multi-granularity and errors of masks. When masks from supervision contain errors (e.g., missing legs of the chair) with multi-granularity (e.g., a small part of the tractor is segmented in a certain view), our correlation shaping successfully addresses these problems and produces correct segmentation masks.

Quality of our 3D labels. We visualize the quality of 3D labels in Fig.13, which are generated using the coarse mask labeling method from Eq.9. As illustrated, these 3D labels are consistent across multiple views (Fig.13(a)) and exhibit high quality (Fig.13(b)) without requiring any optimization.

Regularization loss. During finetuning the attribute decoding network, we introduce an extra regularization loss to help shape the Jacobians. Here Fig. 14 shows the ablation study of this regularization loss. From the area, the area in the red box apparently illustrates the impact of the regularization loss. When perturbing a Gaussian of the tractor, the one with regularization loss can maintains the minimal affects to other objects, while the one without it produces some artifacts to the surroundings. It demonstrates that the regularization loss can better shape the correlation structure of the tangent space of the motion network.

C Proof of Derivation

Given that the attribute decoding networks in neural fields (e.g., NeRFs and 3DGS) are MLPs, we focus on perturbing the weights $W^{(l)}$ of the l-th linear layer in the network $\mathbf{\Phi}_a$ (i.e., $\theta_D = W^{(l)}$), expressed as: $h^{(l)} = W^{(l)}\sigma(h^{(l-1)}) + b^{(l)}$. Let σ denote the non-linear activation function, $b^{(l)}$ be the bias, and $h^{(l)}$ be the (hidden) output of the l-th layer.

To expose the relationship between the gradient of a Gaussian $\mathbf{g}_i$, $\partial\mathbf{\Phi}_i = \frac{\partial\mathbf{\Phi}(f(\mathbf{g}_i);\theta)}{\partial\theta_D}$, and the perturbed weight $W^{(l)}$, we consider the gradient of an arbitrary scalar output z in the attribute decoding network with respect to $W^{(l)}$:

$$z = Y(h^{(l)}) = Y(W^{(l)}\sigma(h^{(l-1)}) + b^{(l)}), \tag{13}$$

(a) Rendered images and corresponding 3D labels generated by coarse mask labeling

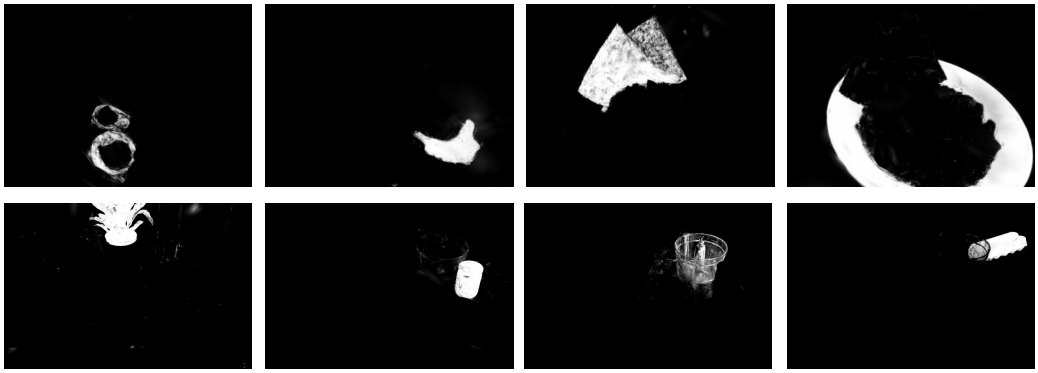

(b) More labels generated by coarse mask labeling

Figure 13: (a) Without any optimization, we produce 3D labels that are consistent across different views. (b) More examples of our 3D labels.done

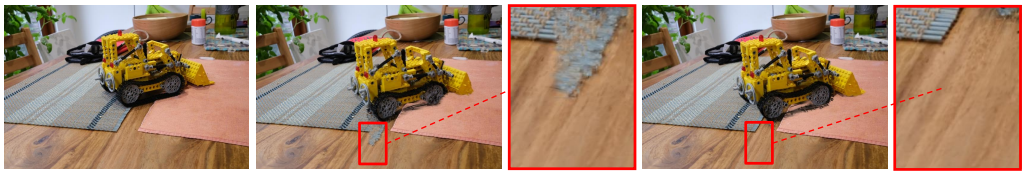

Rendered Image w/o Regularization w/ Regularization

Figure 14: The impact of regularization loss when moving the lego tractor.

where Y denotes all the transformations after l-th layer, z denotes an arbitrary scalar in the vector output of $\mathbf{\Phi}$. Then the differential $\mathrm{d}z$ could be written as:

$$\mathrm{d}z = \frac{\partial z}{\partial h^{(l)}}^{\top} \mathrm{d}h^{(l)} = \sigma(h^{(l-1)}) \frac{\partial z}{\partial h^{(l)}}^{\top} \mathrm{d}W^{(l)} = \mathrm{tr}(\sigma(h^{(l-1)}) \frac{\partial z}{\partial h^{(l)}}^{\top} \mathrm{d}W^{(l)}), \tag{14}$$

as $\mathrm{d}z = \mathrm{tr}(\frac{\partial z}{\partial W^{(l)}}^{\top} \mathrm{d}W^{(l)})$, we could get that:

$$\frac{\partial z}{\partial W^{(l)}} = \frac{\partial z}{\partial h^{(l)}} \sigma(h^{(l-1)})^{\top}, \tag{15}$$

which is a 2D matrix that has the same shape with the $W^{(l)}$. Then the cosine similarity of Jacobians $\partial \mathbf{\Phi}$ between two Gaussians are:

$$\begin{aligned} \cos(\partial \mathbf{\Phi}_i, \partial \mathbf{\Phi}_j) &= \frac{(\frac{\partial z(\mathbf{x}_i)}{\partial h^{(l)}(\mathbf{x}_i)} \sigma(h^{(l-1)}(\mathbf{x}_i))^{\top}) \cdot (\frac{\partial z(\mathbf{x}_j)}{\partial h^{(l)}(\mathbf{x}_j)} \sigma(h^{(l-1)}(\mathbf{x}_j))^{\top})}{\|\partial \mathbf{\Phi}_i\| \|\partial \mathbf{\Phi}_j\|} \\ &= \frac{(\frac{\partial z(\mathbf{x}_i)}{\partial h^{(l)}(\mathbf{x}_i)} \cdot \frac{\partial z(\mathbf{x}_j)}{\partial h^{(l)}(\mathbf{x}_j)})(\sigma(h^{(l-1)}(\mathbf{x}_i))^{\top} \cdot \sigma(h^{(l-1)}(\mathbf{x}_j))^{\top})}{\|\partial \mathbf{\Phi}_i\| \|\partial \mathbf{\Phi}_j\|}, \end{aligned} \tag{16}$$

because $\partial h = \frac{\partial h^{(l)}}{\partial W^{(l)}}$ could be formulated as a 3D tensor, which could be conceptualized as a repeated collection of gradients and each gradient is the vector $\sigma(h^{(l-1)})$. If $\sigma(h^{(l-1)})$ is *well-shaped* satisfying object-level mutual relations (i.e., the absolute value of cosine similarity of $\sigma(h^{(l-1)})$ approaches 1 if $\mathbf{g}_i$ and $\mathbf{g}_j$ belong to the same object, or approaches 0 if not), then ∂h should also satisfy. In this case, if g_i and g_j are affiliated to different objects:

$$\begin{aligned}\cos(\partial\mathbf{\Phi}_i, \partial\mathbf{\Phi}_j) &= \frac{(\frac{\partial z(\mathbf{x}_i)}{\partial h^{(l)}(\mathbf{x}_i)} \cdot \frac{\partial z(\mathbf{x}_j)}{\partial h^{(l)}(\mathbf{x}_j)})(\sigma(h^{(l-1)}(\mathbf{x}_i))^\top \cdot \sigma(h^{(l-1)}(\mathbf{x}_j))^\top)}{\|\partial\mathbf{\Phi}_i\|\|\partial\mathbf{\Phi}_j\|} \\ &= \frac{(\frac{\partial z(\mathbf{x}_i)}{\partial h^{(l)}(\mathbf{x}_i)} \cdot \frac{\partial z(\mathbf{x}_j)}{\partial h^{(l)}(\mathbf{x}_j)})(0)}{\|\partial\mathbf{\Phi}_i\|\|\partial\mathbf{\Phi}_j\|} \\ &= 0,\end{aligned} \tag{17}$$

Eq. 17 indicates that if $\cos(\partial h_i, \partial h_j) = 0$ when g_i and g_j are affiliated to different objects, then $\cos(\partial\mathbf{\Phi}_i, \partial\mathbf{\Phi}_j) = 0$. Meanwhile, $\sigma(h^{(l-1)})$ would not change since the input of $\mathbf{\Phi}_a$ is the fixed $(f(\mathbf{g}_i), d)$. Thus $\cos(\partial h_i, \partial h_j) = 0$ would be consistent during the perturbation. Therefore, we could have the following lemma:

Lemma 1. (*Orthogonality*) After any number of perturbations, the orthogonality of Jacobians between two Gaussians $g_i \in \mathcal{G}_A$ and $g_j \in \mathcal{G}_B$ that are affiliated to different objects ($\mathcal{G}_A \neq \mathcal{G}_B$) would remain consistent:

$$\cos(\partial\mathbf{\Phi}_i^{(d)}, \partial\mathbf{\Phi}_j^{(d)}) = \cos(\partial h_i^{(d)}, \partial h_j^{(d)}) = \cos(\partial h_i^{(0)}, \partial h_j^{(0)}), d \in \mathbb{N}^+, \tag{18}$$

In contrast, we have another lemma:

Lemma 2. (*Similarity*) After any number of perturbations, the similarity of Jacobians between two Gaussians $g_i \in \mathcal{G}_A$ and $g_j \in \mathcal{G}_B$ that are affiliated to the same objects ($\mathcal{G}_A = \mathcal{G}_B$) would remain consistent:

$$\cos(\partial\mathbf{\Phi}_i^{(d)}, \partial\mathbf{\Phi}_j^{(d)}) \approx \cos(\partial h_i^{(d)}, \partial h_j^{(d)}) = \cos(\partial h_i^{(0)}, \partial h_j^{(0)}), d \in \mathbb{N}^+, \tag{19}$$

Proof of Lemma 2: Consider the set of Jacobians $J_A = \{\partial\mathbf{\Phi}_i, g_i \in \mathcal{G}_A\}$ of all Gaussians in an arbitrary object $\mathcal{G}_A$, they all would be orthogonal to the Jacobians of Gaussians from other objects, according to **Lemma 1** if ∂h is *well-shaped*. Thus, the representation space of J_A would be very narrow. If the representation space of $\partial\mathbf{\Phi}$ is compact enough (e.g., the dimension of the representation space of $\partial\mathbf{\Phi}$ is identical to the number of objects in the scene), then the similarity $\cos(\partial\mathbf{\Phi}_i^{(d)}, \partial\mathbf{\Phi}_j^{(d)}) = 1$ when $\mathcal{G}_A = \mathcal{G}_B$. In this extreme case, the set of Jacobians from all the objects in the scene is a group of canonical basis (Bronson, 1969) of the representation space of $\partial\mathbf{\Phi}$.

Combining **Lemma 1** and **Lemma 2**, we could have the conclusion in Eq. 6.